Acta Physica Polonica B Proceedings Supplement **18**, 2-A16 (2025)

STUDY OF PROTON AND NEUTRON EXCITATIONS ALONG SILICON ISOTOPES BETWEEN $N = 20$ AND $N = 28$*

Q. Délignac[a], S. Grévy[a], B. Blank[a], M. Flayol[a], J. Giovinazzo[a] M. Gerbaux[a], A. Husson[a], A. Ortega-Moral[a], A. Barrier[b] E. Clément[b], F. De Oliveira[b], A. Lemasson[b], T. Roger[b] O. Sorlin[b], C. Stodel[b], J.-C. Thomas[b], S. Koyama[b], J. Pancin[b] J. Piot[b], M. Begala[c], S. Calinescu[d], A. Cassisa[e], S. Franchoo[f] H. Jacob[f], M. Juhasz[c], M. Kaci[f], J. Lois-Fuentes[g], J. Michaud[f] J. Mrazek[e], F. Rotaru[d], L. Stanc[d], P. Bednarczyk[h,†] M. Ciemała[h,†], B. Fornal[h,†], I. Matea[f,†], J. Wilson[f,†] O. Stezowski[i,†], M. Lewitowicz[b,†], O. Dorvaux[j,†], S. Kihel[j,†] Ch. Schmitt[j,†], A. Bracco[k,†], S. Brambilla[k,†], F. Camera[k,†] F. Crespi[k,†], S. Leoni[k,†], I. Mazumdar[l,†], V. Nanal[l,†] D. Jenkins[m,†], W. Catford[n,†], M. Stanoiu[d,†], S. Erturk[o,†], J. Gerl[p,†]

[a]LP2iB, Gradignan, France
[b]GANIL, Caen, France
[c]HUN-REN ATOMKI, Debrecen, Hungary
[d]IFIN-HH, Măgurele, Romania
[e]NPI of CAS, Rez, Czech Republic
[f]IJCLab, Orsay, France
[g]USC, Santiago de Compostela, Spain
[h]Institute of Nuclear Physics Polish Academy of Sciences, Kraków, Poland
[i]IP2I Lyon, Villeurbanne, France
[j]IPHC, Strasbourg, France
[k]Milano University, Milan, Italy and INFN, Rome, Italy
[l]TIFR Mumbai, India
[m]University of York, UK
[n]University of Surrey, UK
[o]Nigde University, Turkey
[p]GSI Darmstadt, Germany

Received 9 December 2024, accepted 21 March 2025,
published online 10 April 2025

This paper reports on new $B(\mathrm{E2})$ values for ^{36}Si and ^{38}Si obtained by Coulomb excitation at GANIL during the LISE 2022 campaign. The results agree well with shell model calculations and confirm the increase in proton and neutron excitations in the neutron-rich Si isotopes towards $N = 28$. The experiment was performed in a "brochette" mode together with the ACTAR TPC to measure simultaneously inelastic proton scattering.

DOI:10.5506/APhysPolBSupp.18.2-A16

* Presented at the 57$^{\rm th}$ Zakopane Conference on Nuclear Physics, *Extremes of the Nuclear Landscape*, Zakopane, Poland, 25 August–1 September, 2024.

† For the PARIS Collaboration.

1. Introduction

Light- and medium-masses nuclei are perfect tools to test our understanding of the nuclear structure, in particular, the competition between collective excitations and single-particle properties. Whereas the former ones dominate the structure of stable nuclei in the vicinity of the famous magic numbers (2, 8, 20, 28, 50, 82, and 126), the first ones are essential to correctly describe the properties of nuclei having a number of nucleons away from these magic numbers. All these observations can easily be understood in the framework of a shell structure arising from a one-body central mean field potential created by all the interacting nucleons. In such a picture, magic numbers would be a strong pillar all along the chart of nuclei. Nevertheless, already in the 1960s, anomalies in such a simple global picture were reported with, for example, the unexpected $1/2^+$ ground state of the $N = 8$ ^{11}Be interpreted as arising from additional neutron–proton interaction. In the following decades, evidence for a non-universality of the magic numbers came, first at $N = 20$ from the observation, through the mass measurement of neutron-rich Na isotopes [1, 2], of an unexpected region of deformation, confirmed by the measurement of a low 2^+ excitation energy of ^{32}Mg [3, 4], and finally its high excitation probability $B(\mathrm{E2} : 0^+ \to 2^+)$.

Similar studies [5–7] have shown that another region of deformation develops along the $N = 28$ isotonic chain between the doubly-magic spherical ^{48}Ca ($Z = 20$) and ^{42}Si ($Z = 14$) from which an extremely low 2^+ excitation energy revealed its extremely deformed character despite a semi-magic configuration [8]. Detailed spectroscopic studies have shown that, contrary to $N = 20$ where the deformation arises suddenly between ^{34}Si and ^{32}Mg, the deformation at $N = 28$ gradually develops when protons are successively removed from ^{48}Ca, resulting in various phenomena such as an onset of deformation in ^{46}Ar [9, 10], a prolate-spherical shape coexistence in ^{44}S [11, 12], and a strong oblate configuration in ^{42}Si [8, 13, 14], close to a rigid rotor limit. By comparing the results of these various spectroscopic studies with state-of-the-art shell model calculations, it has been inferred that changes in the structure of the $N = 28$ isotones result from a subtle interplay between neutron excitations above a reduced $N = 28$ shell closure and a proton-induced collectivity due to the degeneracy of the $s_{1/2}$ and $d_{3/2}$ orbitals and a reduced $Z = 14$ sub-shell gap.

The reason for such modifications when protons or neutrons are added to or removed from a nucleus lies in the fact that the nuclear interaction cannot be summarized as a simple one-body central mean field potential but an additional residual nucleon–nucleon interaction has to be considered. In the framework of the shell model in which an appropriate valence space is defined, the different components of the nucleon–nucleon interaction are embedded into the TBME (Two Body Matrix Elements) which account for all the possible degrees of freedom of the valence nucleons such as the spin, isospin, and angular momentum. This effective residual interaction can be decomposed into a monopole part representing the effective single-particle energies and a multipole part which accounts for the correlations, mainly of quadrupole and pairing type. The modification of the shell gaps, which can lead to a disappearance of the magic numbers as observed at $N = 20$ and $N = 28$, is a result of the monopole drift of the nuclear Hamiltonian. Furthermore, Otsuka and collaborators [15, 16] have shown that the tensor component of the residual interaction is of paramount importance to understand the observed evolution of the structure both at $N = 20$ and $N = 28$ shell closures. Indeed, from ^{40}Ca to ^{34}Si, protons and neutrons lie in the *sd* shell, and the $N = 20$ shell closure prevents neutron excitations into the $f_{7/2}$ orbital but the situation changes drastically in ^{32}Mg. When protons are removed from the $d_{5/2}$ orbital, the attractive tensor component between the $d_{5/2}$ protons and the $d_{3/2}$ neutrons is strongly reduced resulting in a much less bound $d_{3/2}$ neutron orbital and, therefore, a reduction of the $N = 20$ gap. At $N = 28$, the proton configuration is slightly different. Indeed, the filling of the neutron $f_{7/2}$ orbital results, again due to the action of the tensor force, in a compression of the $d_{5/2}$–$d_{3/2}$ proton orbitals leading to a near degeneracy of the $d_{3/2}$–$s_{1/2}$ proton orbitals and a reduced $Z = 14$ gap. As a consequence, proton excitations are favored in all $N = 28$ isotones below ^{48}Ca. Moreover, it has been shown that the $N = 28$ shell gap is also progressively reduced when protons are removed from ^{48}Ca by $\approx$ 330 keV/pair of protons, the origin of this reduction being attributed to the tensor and the 2-body spin–orbit interactions. As a consequence, both proton and neutron excitations above $Z = 14$ and $N = 28$ dominate the ground-state structure of ^{42}Si resulting into a strongly oblate shape. Nevertheless, only the beta-decay half-life [17] and the 2^+ and 4^+ excitation energies [8, 13] have been measured so far in ^{42}Si not allowing to extract the relative contribution of proton and neutron excitations.

These contributions can be inferred from the simultaneous measurement of the reduced transition probability B(E2) and the inelastic proton scattering cross section of the 2^+ state as they both, independently, give access to the proton and neutron transition matrix elements M_p and M_n [18] through Eqs. (1) and (2)

$$B(\mathrm{E2}) = (e_p M_p + e_n M_n)^2 \,, \tag{1}$$

$$\frac{M_n}{M_p} = \frac{1}{3}\left[\frac{\delta_{pp'}}{\delta_{\mathrm{CoulEx}}}\left(1 + 3\frac{N}{Z}\right) - 1\right] , \tag{2}$$

where e_p (e_n) is the proton (neutron) effective charge, $\delta_{pp'}$ and δ_{CoulEx} are the deformation lengths proportional to the proton inelastic scattering and Coulomb excitation cross sections, respectively.

In the following, we will report on the first results of an experiment performed at GANIL in order to study the evolution of the proton and neutron excitations in the 2^+ states of neutron-rich Si isotopes between the $N = 20$ and $N = 28$ shell closures.

2. The experiment

As explained before, the relative contribution of protons and neutrons to the excitation of the 2^+ excited state in a nucleus can be obtained through the measurement of both proton inelastic scattering and Coulomb excitation processes. Therefore, an experiment (E823) has been performed in 2022 at GANIL (Grand Accelerateur National d'Ions Lourds) using the LISE (Ligne d'Ions Super Epluchés) spectrometer to produce and select the exotic ^{34,36,38}Si isotopes. Their proton inelastic scattering cross sections and $B(\mathrm{E2} : 0^+ \to 2^+)$ values have been measured using two independent setups, the first one being "transparent", allowing these measurements to be done simultaneously using the same secondary beam ("brochette" mode).

The first setup was the ACTAR TPC detector (ACtive TARget Time Projection Chamber) filled with 10% isobutane and 90% dihydrogen at a pressure of 950 mbar, corresponding to an effective thickness of 6 mg/cm^2. Low-energy scattered protons up to $\sim$ 3 MeV were stopped in the gas, whereas protons with higher energy up to $\sim$ 10 MeV were stopped in an array of 20 Si detectors located on both sides of ACTAR TPC. The scattering angles were determined from the proton traces in the gas. The results obtained with the ACTAR TPC detector are not part of the work presented here and, therefore, the setup and the first results for the Coulomb excitation will be presented in the following.

The secondary beam that did not react in the gas of ACTAR TPC was collected and refocused by a set of quadrupoles into the second setup dedicated to the Coulomb excitation measurement (Fig. 1). In order to measure the position, energy, and timing of the incoming and diffused nuclei, several Si and gas detectors were used, whereas gamma rays were detected using HPGe and scintillators detectors. The (ΔE, ToF) identification of incoming particles was done on an event-by-event basis (ΔE was measured with the ionization chamber CHIO and the time of flight was obtained using the gaseous detectors CATS D4 and CFA separated by a distance of $\sim$ 23 meters), whereas their trajectories were measured by the gaseous position-sensitive detectors CATS1 and CATS2 separated by $\sim$ 0.5 meters. The gamma detection located around the CoulEx target (Au with an effective thickness of 400 mg/cm^2) was composed of 8 PARIS clusters (NaI-LaBr3/CeBr3 Phoswichs) and 8 EXOGAM HPGe clovers. After the target, the nuclei were identified by (ΔE, E) measurements done using the newly developed Zero Degree Detector (ZDD) between 0 and ~ 3 degrees and two Double-sided Silicon Strip Detectors (DSSD) from ~ 3 and ~ 7.6 degrees. The ZDD is composed of a set of 2 drift chambers for X–Y positions, 5 ionization chambers for ΔE, and 5 plastics for E measurements.

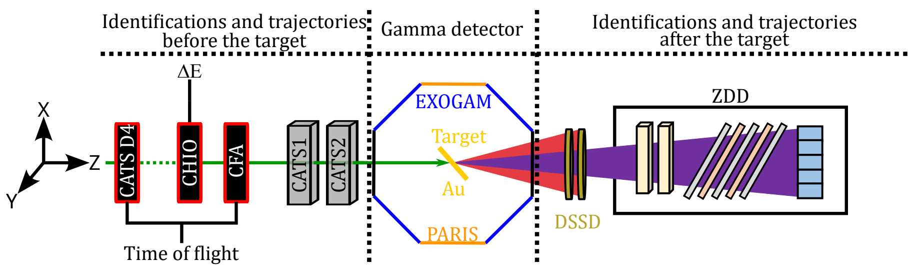

Fig. 1. Scheme of the CoulEx setup.

3. Analysis and preliminary results

The detection of gamma rays from the Coulomb excitation in coincidence with nuclei gives access to the experimental cross section defined as follows:

$$\sigma = \frac{N_\gamma}{N_{\mathrm{inc}}} \times \frac{M_{\mathrm{Au}}}{N_{\mathrm{A}}\,\rho_{\mathrm{Au}}\,d_{\mathrm{Au}}}\,, \tag{3}$$

with N_γ the number of gamma-rays, N_{inc} the number of incoming nuclei, N_{A} Avogadro constant, and ρ_{Au} volumic mass, M_{Au} molar mass, d_{Au} thickness of the gold target. For a preliminary analysis, the $B(\mathrm{E2})_X$ value can be extracted using a reference nucleus with a known $B(\mathrm{E2})_{\mathrm{ref}}$ value defined as

$$\frac{B(\mathrm{E2})_X}{B(\mathrm{E2})_{\mathrm{ref}}} \propto \frac{\sigma_X}{\sigma_{\mathrm{ref}}} \tag{4}$$

with σ_X (σ_{ref}) being the cross section of the interest nucleus (of the reference nucleus). This method is valid under the condition that both nuclei are detected under the same experimental conditions and, therefore, we chose as reference nucleus transmitted in the same setting as the nucleus of interest. As can be seen from Fig. 2, the sulfur isotopes, for which the $B(\mathrm{E2})$ values are well known [12], were transmitted to our settings. Therefore, the $B(\mathrm{E2})$ of ^{38}Si will be determined relative to the one of ^{42}S (black and red/gray cuts in Fig. 2, left, respectively), whereas for ^{36}Si, the reference nucleus is ^{40}S. In order to select inelastically scattered nuclei after the target, a selection is applied on the (ΔE, E) plot, as shown in Fig. 2, right for the Si (black) and S (red/gray) isotopes.

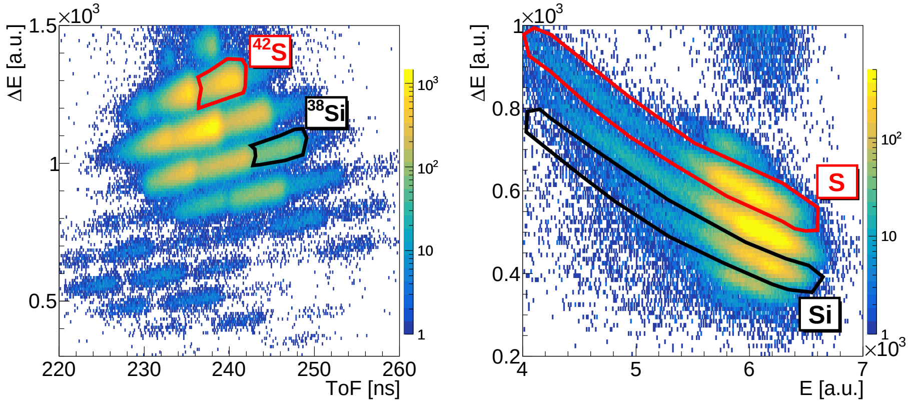

Fig. 2. (Color online) Identification and possible nucleus selection with a setting centered on ^{38}Si. Left panel: (ΔE, ToF) identification for all transmitted nuclei and selection before target with ^{42}S (red/gray) and ^{38}Si (black) contours. Right panel: (ΔE, E) scattered nucleus identification after target with contours on S (red/gray) and Si (black) isotopes. Note that no selection on the incoming nuclei is done for the (ΔE, E) plot.

In order to extract reliable B(E2) values, it is important to not take into account nuclear excitations that will occur for small impact parameters, such a selection being ensured by restricting the deflection angles below a “safe” value that depends on the experimental conditions. In our case, we have used the DWEIKO calculations to estimate the “safe” angles (see Fig. 3) for ^{42}S and ^{38}Si). The maximum of the nuclear contribution is found around 4.5° (in the laboratory frame) and, therefore, the results presented in the following will be obtained by selecting the nuclei deflected at angles below 2.5°.

The Doppler-corrected gamma-ray spectra for ^{42}S (red/left panels) and ^{38}Si (blue/right panels) obtained with EXOGAM and PARIS under the conditions discussed above are shown in Fig. 4. The ($0^+ \rightarrow 2^+$) transition at 903 keV for ^{42}S and 1078 keV for ^{38}Si are clearly visible. The same analysis has been performed on ^{40}S (red/left panels) and ^{36}Si (blue/right panels) with transitions at 903 and 1436 keV, respectively (see Fig. 5). The gamma-ray efficiency curve has been determined using standard ^{60}Co, ^{152}Eu, and ^{207}Bi sources and efficiencies of 3.8(2)% and 6.0(3)% have been determined at 1 MeV for EXOGAM and PARIS, respectively. The independent analysis performed on both gamma spectrometers showing perfect consistency after

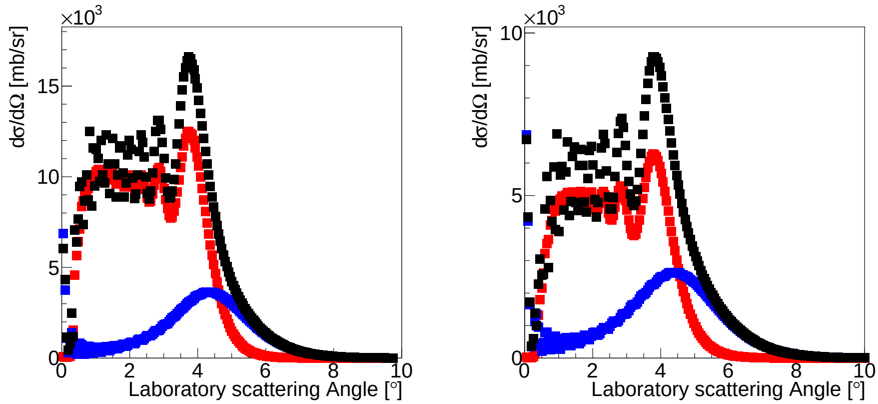

Fig. 3. (Color online) Angular distribution of ^{42}S (left panel) and ^{38}Si (right panel) calculated by DWEIKO with the Coulomb and nuclear cross sections (black squares), only the Coulomb cross section (red/light gray squares), and only the nuclear cross section (blue/gray squares).

gamma efficiency correction, allows us to use the mean value from EXOGAM and PARIS as the final gamma-ray number in order to determine the B(E2) values.

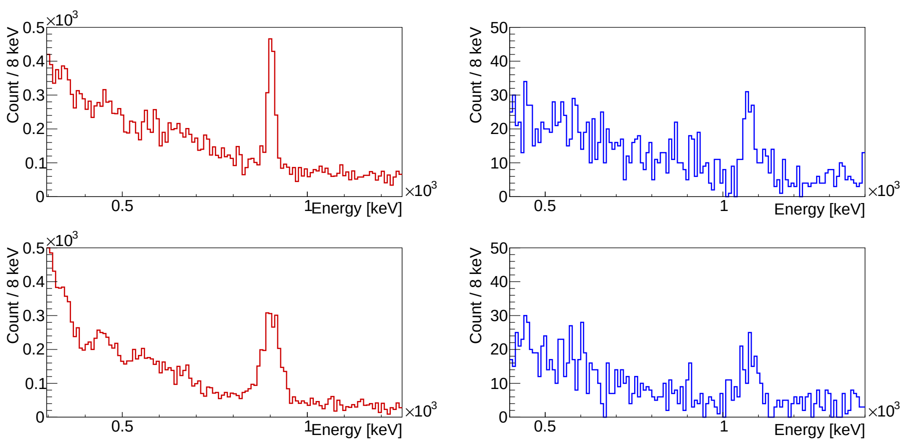

Fig. 4. (Color online) Doppler-corrected gamma energy spectra of ^{42}S (red, left panels) and ^{38}Si (blue, right panels) with a gate on angles below 2.5°. Top panels: EXOGAM; Bottom panels: PARIS.

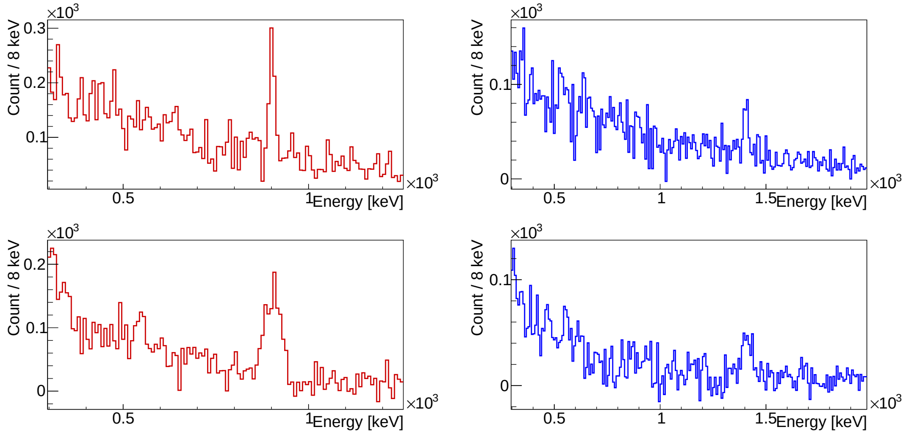

Fig. 5. (Color online) Doppler-corrected gamma energy spectra of ^{40}S (red, left panels) and ^{36}Si (blue, right panels) with a gate on angles below 2.5°. Top panels: EXOGAM; Bottom panels: PARIS.

The preliminary $B(\mathrm{E2})$ values obtained in this work are given in Table 1 together with the literature ones [19] and shell model predictions obtained using the SDPF-U [20, 21] interaction, which is known to well describe the evolution of the structure in the neutron-rich $N = 28$ isotopes. Despite an analysis which is not definitive, the new values agree with the previous ones within the uncertainties that have been significantly reduced. In addition, the new results seem to favor an increase in the $B(\mathrm{E2})$ values of the order of $\sim 20\%$ between ^{36}Si and ^{38}Si, as predicted by the shell model. It is, therefore, consistent with an increase in proton and neutron excitations in Si isotopes towards $N = 28$, the $B(\mathrm{E2})$ values of ^{40}Si and ^{42}Si being predicted to be 360 $e^2\mathrm{fm}^4$ and 535 $e^2\mathrm{fm}^4$, respectively.

Table 1. $B(\mathrm{E2})$ values for ^{36}Si and ^{38}Si.

$B(\mathrm{E2},\uparrow)$ [$e^2\mathrm{fm}^4$]	This work	SDPF-U [21]	Ref. [19]
^{36}Si	220(26)	205	193(59)
^{38}Si	244(40)	245	193(71)

4. Conclusion and outlook

New $B(\mathrm{E2})$ values obtained at GANIL have been reported for ^{36}Si and ^{38}Si. The preliminary results seem to favor the increase in proton and neutron excitations towards $N = 28$ under the action of the tensor force that reduces both the $Z = 14$ and $N = 28$ shell gaps. More precise results for the $B(\mathrm{E2})$ values and the analysis of the ACTAR TPC data obtained during the same experimental campaign will allow us to extract independently proton and neutron contributions to the 2^+ state and, therefore, will provide a better comparison with theoretical predictions.

REFERENCES

[1] C. Thibault *et al.*, *Phys. Rev. C* **12**, 644 (1975).
[2] X. Campi, H. Flocard, A.K. Kerman, S. Koonin, *Nucl. Phys. A* **251**, 193 (1975).
[3] C. Détraz *et al.*, *Phys. Rev. C* **19**, 164 (1979).
[4] D. Guillemaud-Mueller *et al.*, *Nucl. Phys. A* **426**, 37 (1984).
[5] O. Sorlin, M.-G. Porquet, *Phys. Scr.* **2013**, 014003 (2013).
[6] L. Gaudefroy *et al.*, *Phys. Rev. Lett.* **97**, 092501 (2006).
[7] A. Gade *et al.*, *Phys. Rev. C* **74**, 034322 (2006).
[8] B. Bastin *et al.*, *Phys. Rev. Lett.* **99**, 022503 (2007).
[9] A. Gade *et al.*, *Phys. Rev. C* **68**, 014302 (2003).
[10] S. Calinescu *et al.*, *Phys. Rev. C* **93**, 044333 (2016).
[11] T. Glasmacher *et al.*, *Phys. Lett. B* **395**, 163 (1997).
[12] B. Longfellow *et al.*, *Phys. Rev. C* **103**, 054309 (2021).
[13] S. Takeuchi *et al.*, *Phys. Rev. Lett.* **109**, 182501 (2012).
[14] A. Gade *et al.*, *Phys. Rev. Lett.* **122**, 222501 (2019).
[15] T. Otsuka *et al.*, *Phys. Rev. Lett.* **87**, 082502 (2001).
[16] Y. Utsuno *et al.*, *Phys. Rev. C* **86**, 051301 (2012).
[17] S. Grévy *et al.*, *Phys. Lett. B* **594**, 252 (2004).
[18] A.M. Bernstein, V.R. Brown, V.A. Madsen, *Phys. Lett. B* **103**, 255 (1981).
[19] R.W. Ibbotson *et al.*, *Phys. Rev. Lett.* **80**, 2081 (1998).
[20] Y. Sun *et al.*, *Phys. Lett. B* **802**, 135215 (2020).
[21] F. Nowacki, private communication.